physica status solidi rrl
www.pss-rapid.com

Stable Molybdenum Nitride Contact for Efficient Silicon Solar Cells

Yajuan Li, Yuxiong Li, Guohua Zhang, Jingye Li, Dong Liang, Yanfei Wu, Tao Song, Xinbo Yang, Dongdong Li, Chunping Jiang, and Baoquan Sun**

Carrier-selective passivating contacts play a crucial role in highly efficient silicon solar cells targeting the cost-effective photovoltaic industry. Widely developed hole-selective passivating-contact molybdenum oxide (MoO_x) exhibits inferior long-term stability induced by chemical reactions between the MoO_x and the adjacent metals. Herein, low-temperature magnetron-sputtering-deposited molybdenum nitride (MoN_x) films are developed as stable hole-selective passivating contacts for crystal silicon solar cells. The work function of the MoN_x films can be as deep as 5.62 eV featuring a low resistivity of $5.0 \times 10^{-4}\,\Omega$ cm by optimizing the deposition process. Quasi-metallic MoN_x integrated with a MoO_x passivating layer is verified to act as effective hole-selective passivating contacts for crystal silicon solar cells, yielding a power convertion efficiency (PCE) above 17%. Although the hole-selective passivation of MoN_x films is inferior to fresh MoO_x ones, the device performance with MoN_x film is kept stable with time in air exposure and surpasses MoO_x films after 6 months. The stable performance is ascribed to the metal electrodes diffusion barrier and insusceptible work function of MoN_x films compared to MoO_x films. This work makes a preliminary exploration to develop efficient crystal silicon solar cells with stable and cost-effective metal nitrides as hole-selective passivating contacts.

1. Introduction

Crystalline silicon (c-Si) solar cells with heavily doped and directly metalized contact dominate the world photovoltaic (PV) market, but their efficiency is mainly limited by the high carrier recombination loss caused by a high density of electronically active states at the metal–silicon contact regions.[1] Compared to aluminum back surface field (Al-BSF) cell, passivated emitter and rear cells (PERCs) can improve the upper limit of power conversion efficiency (PCE) from 20% to 24% through decreasing the metal–silicon contact areas and passivating the noncontacted areas of silicon surface with insulating dielectric layers including silicon nitride (SiN_x) or Al_2O_3/SiN_x stacks.[2] In addition to metal–silicon contacts, the heavily doped silicon used for selectively collecting electrons and holes limits the device efficiency by notably Auger recombination,[3] bandgap narrowing, and free-carrier absorption.[4] Also, a high-temperature-doping process burdens fabrication complexity further. To push the PCE close to the limit of 29.4%[5] and simplify the fabrication process, whole area carrier-selective passivating heterocontacts are becoming mainstream for the PV industry. As archetypal examples, heterojunction with intrinsic thin layer (HIT) solar cells using intrinsic hydrogenated amorphous silicon (a-Si:H) as surface passivation and p/n-doped a-Si:H as hole/electron-selective contacts achieved a record efficiency of 25.1% and 26.7% with interdigitated back contact (IBC),[6] and tunnel-oxide passivating contact (TOPCon) solar cells with thermal SiO_2 as surface passivation and doped poly-Si as carrier-selective contacts can achieve an efficiency of 25.7% and 26.1% with IBC structure.[7] Nonetheless, the i/p- or i/n-doped a-Si:H stacks are deposited by plasma-enhanced chemical vapor deposition (PECVD), a capital-intensive system employing flammable and toxic

Dr. Y. Li, G. Zhang, D. Liang, Y. Wu, Dr. T. Song, Prof. D. Li, Prof. B. Sun
Jiangsu Key Laboratory for Carbon-Based Functional Materials & Devices
Institute of Functional Nano & Soft Materials (FUNSOM)
Soochow University
Suzhou 215123, P. R. China
E-mail: bqsun@suda.edu.cn

Y. Li, Prof. C. Jiang
Key Lab of Nanodevices and Applications
Suzhou Institute of Nano-Tech and Nano-Bionics
Chinese Academy of Sciences (CAS)
Suzhou 215123, P. R. China
E-mail: cpjiang2008@sinano.ac.cn

The ORCID identification number(s) for the author(s) of this article can be found under https://doi.org/10.1002/pssr.202100159.

J. Li, Prof. D. Li
CAS Key Lab of Low-Carbon Conversion Science and Engineering
Shanghai Advanced Research Institute
Chinese Academy of Sciences
99 Haike Road, Zhangjiang Hi-Tech Park, Pudong, Shanghai 201210, P. R. China

Prof. X. Yang
College of Energy
Soochow University
Suzhou 215006, P. R. China

Prof. B. Sun
Macau Institute of Materials Science and Engineering
Macau University of Science and Technology
Taipa, Macau SAR 999078, P. R. China

DOI: 10.1002/pssr.202100159

boron/phosphorous gas precursors. In this sense, risk-free materials deposited at low temperatures and providing carrier-selective passivating contacts comparable to the dopant-diffused n^+ and p^+ silicon are highly desirable.[8]

Based on the aforementioned consideration, transition metal oxides or conductive polymers with a broader range of work functions, prepared using simple, low-temperature physical vapor deposition or even solution-based processing techniques, have been applied on c-Si solar cells as carrier-selective layers. In general, carrier selectivity is inferred from the band bending induced on the Si surface, which depends on the valence and conduction band edges and the work function of the material. The low-work-function materials, for example, titanium oxides (TiO_x),[9] tantalum oxides (TaO_x), and magnesium oxides (MgO_x),[10] have been demonstrated on c-Si solar cells to be suitable for electron-selective contacts through inducing downward band bending on the Si surface. Materials with large work function such as vanadium oxides (VO_x),[11] molybdenum oxides (MoO_x),[12] tungsten oxides (WO_x), and poly(3,4-ethylenedioxythiophene): polystyrene sulfonate (PEDOT:PSS) were experimentally confirmed to pull Si band bend upward, therefore, reducing the hole injection barrier at the interface.[13] Yet, PEDOT:PSS is chemically unstable in the air and suffers from photodegradation.[14] MoO_x and VO_x are reported to be sensitive to adventitious carbon and water adsorption upon air exposure.[15] The work function of the MoO_x surface can change from 6.8 to 5.3 eV by gradually exposure to air.[15c] The reactions at the Si/MoO_x and MoO_x/metals interface will induce decreased metal oxidation state and reduced work function,[16] and the annealing process will accelerate the change of interface states.[17] The sensitivity of metal oxides leads to unstable device performance and complex influencing factors,[18] making alternative carrier-selective passivating contacts with inert properties more attractive.

Given the appropriate work function, excellent conductivity, superior chemical, and physical stability, transition metal nitrides were considered to be potential carrier-selective passivating contacts on c-Si solar cells in recent years. Titanium nitrides (TiN_x)[19] and tantalum nitrides (TaN_x)[20] were confirmed to be excellent electron-selective layers on c-Si solar cells achieving PCE above 20% and high stability. There are few reports about hole-selective passivation on c-Si solar cells based on transition metal nitrides. Molybdenum nitrides (MoN_x) thin film showed high hardness, excellent electrical conductivity, and superior chemical resistance, which give it various applications such as hard coatings, gate electrodes, diffusion barriers, and catalysts.[21] The work function of MoN_x can be deep enough to 5.33 eV,[22] which is close to the position of valence band maximum of silicon located at 5.1 eV, making it a potential hole-selective passivating contact on c-Si solar cells.

Here, low-temperature magnetron sputtering deposited MoN_x films exhibiting high work function and excellent conductivity were developed as regular hole-selective passivating contact for c-Si solar cells. The work function of the quasi-metallic MoN_x layer can achieve a value as deep as 5.62 eV with a low resistivity of $5.0 \times 10^{-4}\,\Omega\,\mathrm{cm}$. The open-circuit voltage (V_{oc}) and fill factor (FF) of devices increased with MoN_x film thickness. At last, the PCE of devices with MoN_x as hole-selective passivating contact can reach near 16% and exhibited excellent stability than devices without MoN_x film. The MoN_x film combining with a MoO_x passivating layer acted as an effective hole-selective passivating contact for crystal silicon solar cells, which delivered a PCE of above 17% and enhanced device stability than a single MoO_x passivating layer. Our work provides a strategy to explore stable and cost-effective metal nitride as hole-selective passivating contact instead of widely developed metal oxides for efficient crystal silicon solar cells.

2. Results and Discussion

2.1. Physical and Chemical Characterization of MoN_x Films

A series of MoN_x films were deposited by magnetron sputtering of molybdenum targets in a mixed carrier gas of N_2 and Ar. Different gases with N_2:Ar ratios varying from 1:5, 1:3, 1:2, to 1:1 and different sputtering powers varying from 40 W, 60 W, to 100 W were used to modulate the resistivity of MoN_x films. Specific information about these films is summarized in Table S1, Supporting Information, (N_2:Ar ratios) and Table S2, Supporting Information (powers). The resistivity of MoN_x reduced with decreasing nitrogen gas concentrations at the same sputtering power (60 W), a trend also observed by previously reported work,[23] as shown in **Figure 1**a. MoN_x exhibits a close-packed metallic structure in which nitrogen atoms present in interstitial sites.[21a] As the number of nitrogen atoms in MoN_x films ascended, the increased scattering of electrons due to nitrogen between the metal atoms was bound to render lower mobility than that in the pure metal, and more nitrogen atoms induced higher resistivity. By increasing the sputtering power from 40 to 100 W with N_2:Ar ratio of 1:3, the resistivity of MoN_x dropped from 1.1×10^{-3} to $5.0 \times 10^{-4}\,\Omega\,\mathrm{cm}$. X-ray diffraction (XRD) spectra (Figure S1, Supporting Information) revealed that the MoN_x films were amorphous at lower sputtering power, and the Mo_2N crystal phase emerged when sputtering power reached 100 W. The improved conductivity should be correlated with the enhanced crystallinity as the sputtering power growing. Although the film quality of MoN_x prepared at 100 W with the sputtering equipment cannot be easily controlled, it sometimes showed a rough surface observed by the naked eye. This may be correlated with the rapid crystallization induced by high sputtering power and limited further increasing the sputtering power in this work. The work function obtained from ultraviolet photoelectron spectroscopy (UPS) of the MoN_x films can be modulated from 5.39 eV (N_2:Ar = 1:1) to 5.62 eV (N_2:Ar = 1:5) (Figure 1b). These values are higher than the reported 5.33 eV of MoN film,[22] which is ascribed to the different compositions of films and the different methods to extract work function value.

The chemical composition of amorphous MoN_x films was also investigated by X-ray photoelectron spectroscopy (XPS). Considering the diverse valence states of Mo in amorphous MoN_x films, the Mo3d peaks were fitted by three kinds of Mo states including Mo—O bond with the binding energy of $Mo3d_{5/2}$ at 232.60 eV, Mo—N bond with a higher binding energy of $Mo3d_{5/2}$ at 230.17 eV, and Mo—N bond with a lower binding energy of $Mo3d_{5/2}$ at 229.09 eV, as shown in Figure 1c. The atom percentage variation of the three kinds of Mo with nitrogen gas concentrations is summarized in Table S3, Supporting Information. Mo—O bond content ratio kept constant with a

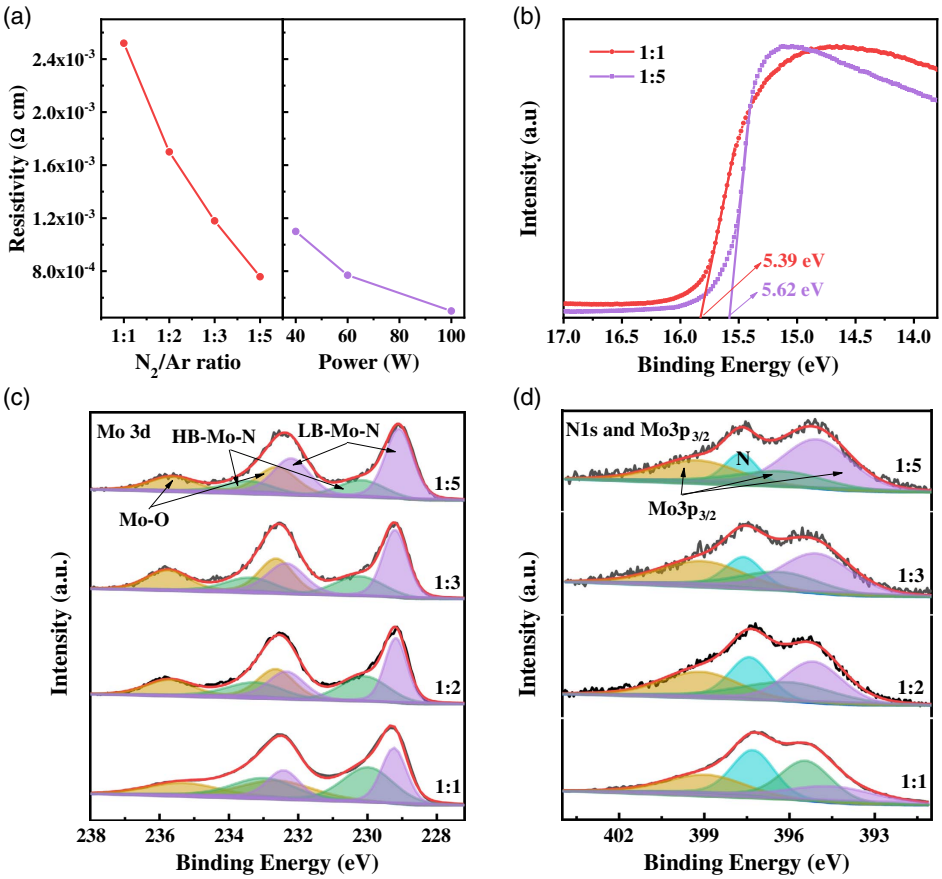

Figure 1. The resistivity, work-function, and compositions of MoN_x film prepared by magnetron sputtering method. a) The resistivity of MoN_x films prepared at different N_2/Ar ratios (with sputtering power of 60 W) and different sputtering powers (under N_2/Ar ratio of 1:3). b) Work functions of MoN_x films (prepared under N_2/Ar ratios of 1:1 and 1:5 with sputtering power of 60 W) obtained by UPS measurements. c) Mo 3d core levels of amorphous MoN_x films prepared at different N_2/Ar ratios and d) corresponding evolution of overlapped peaks of N 1s and Mo $3p_{3/2}$ core levels.

value of ≈30%, Mo—N bond with lower binding energy elevated its ratio from 30% to 50% whereas Mo—N bond with higher binding energy degraded its ratio from 40% to 20% when nitrogen gas proportion decreased. Based on the aforementioned percentage variation, the Mo—O bond should be ascribed to MoO_x formed in MoN_x film. The origin of the O in the Mo—O bond was proposed to be ascribed to the oxygen in the N_2 and Ar gas flow and the oxygen remaining in the vacuum chamber during deposition, which is also reported in the deposition of TiN_x films.[24] A constant oxygen signal was detected through the whole MoN_x film in time-of-flight secondary-ion mass spectrometry (ToF-SIMS), as shown in Figure S2, Supporting Information, which confirmed the O in the Mo—O bond was not just from adventitious oxygen contamination. In addition, the valence state of Mo in the Mo—N bond varied with nitrogen gas proportion, which will affect the conductivity and work function of MoN_x films, as similar as MoO_x films.[15a] The N1s peak is overlapped with Mo$3p_{3/2}$ peaks in binding energy spectra. Mo$3p_{3/2}$ peaks were fitted by three kinds of Mo states based on the atom ratios obtained from Mo3d peaks, and the fitting results in overlapped peaks of N1s and Mo$3p_{3/2}$ are shown in Figure 1d. The N/Mo ratios of amorphous MoN_x film were calculated with peak areas of N1s and Mo$3d_{5/2}$ peaks and declined from 0.88 to 0.51 with decreasing nitrogen gas proportion (Table S3, Supporting Information). This confirmed that resistivity of amorphous MoN_x film is positively proportional to the nitrogen concentration in the film. In other metal nitride films such as TiN_x, the increasing resistivity with growing nitrogen concentration is attributed to the decrease in the cubic TiN phase in the films.[24] Here, higher nitrogen concentration results in growing amounts of Mo with a higher valence state, which is not similar to the situation in TiN_x films.

2.2. Devices with MoN_x as Hole-Selective Passivating Contacts

Considering the superior conductivity and appropriate work function of MoN_x films, whole area rear MoN_x/Ag hole-selective passivating contacts on devices that have the same front structures as industrial p-type PERCs (**Figure 2**a) were studied. The best device with MoN_x film (prepared at 60 W under N_2:Ar ratio of 1:5 for 10 min) rendered a PCE of 15.9% featuring a V_{oc} of 0.594 V, a FF of 78.91%, and a J_{sc} of 34.14 mA cm^{-2} (Figure 2b and Table S4, Supporting Information). When tuning the deposition power from 60 to 100 W or changing the N_2:Ar

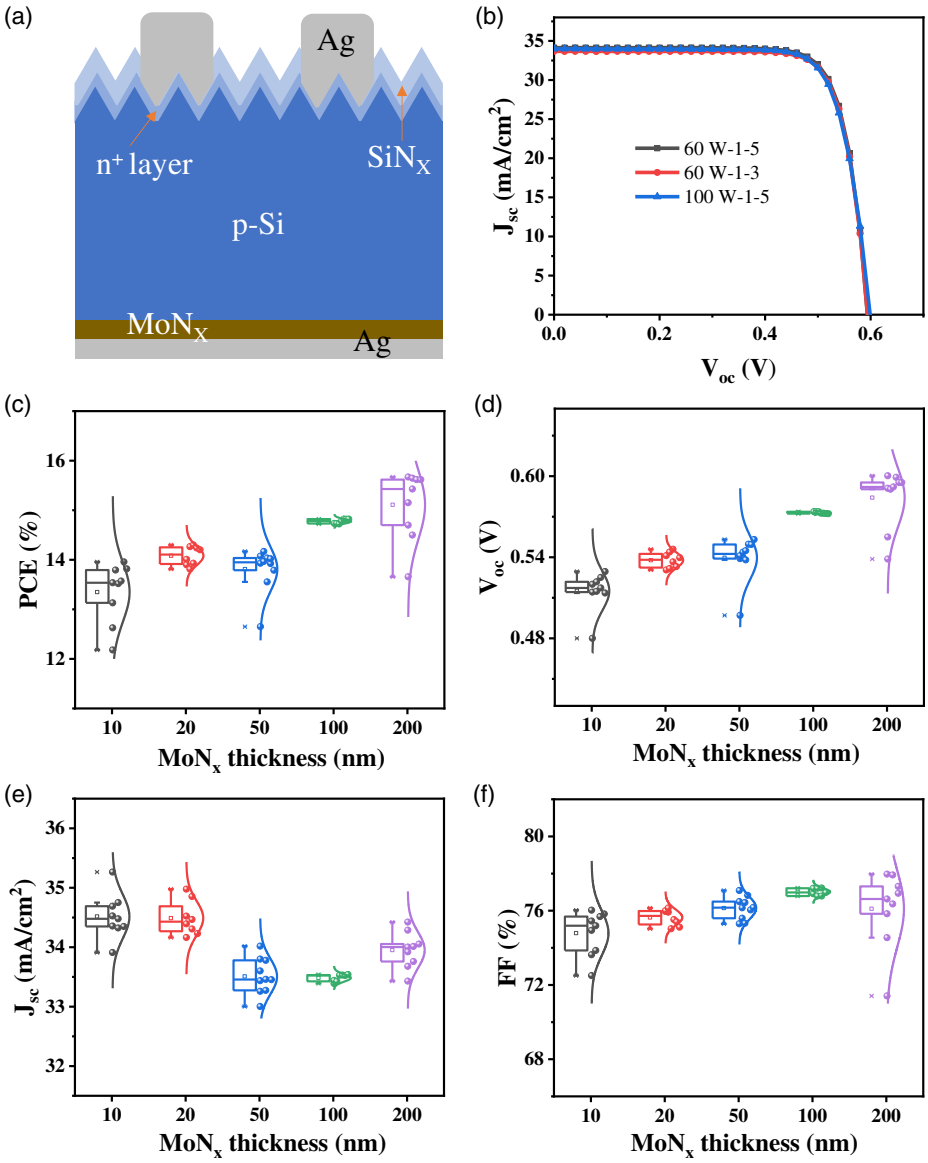

Figure 2. The performance of devices with MoN_x film as hole-selective passivation contacts. a) The diagram of the device structure. b) *J–V* curves of devices with MoN_x film prepared at N_2/Ar ratio of 1:5 or 1:3 and sputtering power of 60 or 100 W, termed as 60 W-1-5, 60 W-1-3, and 100 W-1-5. c) The PCE, d) V_{oc}, e) J_{sc}, and f) FF of the devices with different thicknesses of MoN_x films.

ratio from 1:5 to 1:3, the PCE values showed slight difference. The results indicated that the performance of the devices was insensible to the work function or conductivity change in a specific range. According to the thickness information in Table S2 and S5, Supporting Information, the film deposited at 100 W for 10 min (≈300 nm) is thicker than 60 W (≈200 nm). The thickness beyond 200 nm would have a negligible impact on PCE. At N_2/Ar ratio of 1:5 and sputtering power of 60 W, the device performances with different thicknesses (below 200 nm) of MoN_x films are also summarized in Figure 2c–f. With increasing the MoN_x film thickness from 10 to 200 nm, the PCE of the device gradually elevated from ≈14% to ≈16% (Figure 2c). The improved PCE for the device with a thicker MoN_x film was correlated with increased V_{oc} (Figure 2d) and FF (Figure 2f), which manifested that a thicker MoN_x film can provide better hole transportation and suppression of electron recombination. The suppression of electron carrier recombination at the Si/MoN_x interface would enhance the V_{oc}, and the series resistance hindering the collection of hole carriers would deteriorate the device FF.[2] Although a thicker MoN_x film would result in J_{sc} recession (Figure 2e). External quantum efficiency (EQE) in the long-wavelength range (from 970 to 1100 nm) also degraded with increasing film thickness, as shown in Figure S3a, Supporting Information, which is likely ascribed to the parallel light absorption of MoN_x films (Figure S3b, Supporting Information). The intense light absorption of MoN_x film mainly arises from free carrier absorption as similar as TiN_x film.[19] The Hall effect measurement showed the carrier density in MoN_x

films was as high as $10^{23}\,cm^{-3}$ (Table S6, Supporting Information), the same order of magnitude with reported TiN_x films,[19] which confirmed free carrier absorption and quasi-metal property of MoN_x film. The minor carrier effective lifetime (τ_{eff}) of silicon wafers (1 Ω cm, double faces-polished) passivated with MoN_x films on the rear side was characterized to confirm the passivation of MoN_x on silicon and summarized in Table S7, Supporting Information. Thicker MoN_x film (200 nm) with τ_{eff} of 10.7 μs induced better passivation than thinner MoN_x (10 nm) with τ_{eff} of 9.5 μs, which confirmed that thicker MoN_x film showed higher V_{oc}. While compared to τ_{eff} (10.4 μs) of silicon wafer without any passivation film, τ_{eff} improvements are so tiny that the passivation of MoN_x films on the silicon surface is weak.

Because of inferior passivation on silicon, devices with MoN_x films yielded a lower PCE than with commonly reported hole-selective passivating MoO_x films. As shown in Table S4, Supporting Information, the MoO_x passivated device can yield a PCE of 17.7% with an improved V_{oc} of 0.630 V and a J_{sc} of 36.60 mA cm^{-2}. The silicon surfaces passivated by MoO_x films were reported to show much higher τ_{eff} (≈20 μs) than bare silicon surface (≈8 μs).[25] The specific contact resistances of MoN_x/Si and MoO_x/Si contact were also characterized using the Cox and Strack method.[26] The current density–voltage (J–V) curves of Ag/MoN_x/Si/Al structure are not ohmic contact as Ag/MoO_x/Si/Al structure, which exhibited rectifying behaviors that favored hole-transporting from p-type silicon to MoN_x films. So the specific contact resistances were just estimated based on the resistance at lower voltages between −0.1 and 0.1 V (Figure S4, Supporting Information). The fitted contact resistivity (1.38 Ω cm^2) of MoN_x/Si contact is 6.5 times larger than that (0.211 Ω cm^2) of MoO_x/Si one. The larger electrical contact resistance between MoN_x and silicon also leads to lower device performance than MoO_x.

The enhanced hole-selective passivation of MoO_x was related to its higher work function than MoN_x because higher work function would further reduce hole transport barrier according to Schottky–Mott theory. In addition to band bending upward at silicon surface induced by high work function, the formation of hole-selective contacts is also correlated with surface dangling bonds, metal-induced gap states, and interface dipoles.[27] The passivation of MoO_x on Si was attributed to a reactive Si–O interlayer formed by the chemical reaction between oxygen in MoO_x and Si.[16b] A weak passivation effect of MoN_x may be related to the absence of the reactive Si–O interlayer that passivates the Si dangling bonds. The MoO_x/Si and MoN_x/Si interfaces were characterized by ToF-SIMS analysis. As shown in Figure S5, Supporting Information, a thicker SiO_x layer was detected at the MoO_x/Si interface than MoN_x/Si interface. At last, the quasi-metal property of MoN_x likely generated gap states at Si/MoN_x interface, as similar as metals, leading to inferior passivation and nonohmic contact.

2.3. Stable MoN_x Hole-Selective Passivating Contact

Although the passivation effect of MoN_x on c-Si is modest, we found that the Si/MoN_x/Ag contact showed superior stability. As shown in **Figure 3**a–d, PCE, V_{oc}, J_{sc}, and FF of the devices with MoN_x (200 nm)/Ag rear contacts were tracked for ≈7 months in ambient conditions. The stable PCEs of devices with MoN_x/Ag rear contacts were observed, which mainly contributed from the stable V_{oc} and improved FF. The devices with a thinner MoN_x film showed the same stability. The PCE of the devices with MoN_x (10 nm)/Ag, MoN_x (20 nm)/Ag, and MoN_x (50 nm)/Ag contacts changed from 13.5%, 14.0%, and 14.2% to 14.0%, 14.3%, and 14.3% after 6 months. The low solubility of metal in MoN_x builds a stable barrier to prevent silver atoms from diffusing or interacting with silicon,[21] avoiding unstable Si/Ag contacts.[28] In a word, MoN_x films provide both insensitive interfaces of Si/MoN_x and MoN_x/Ag, leading to the devices with MoN_x films yielding stable PCE. Unfortunately, the instability of the MoO_x/Ag interface induced severe performance degradation of devices with MoO_x/Ag contacts, as shown in Figure 3e,f. MoO_x generally shows poor conductivity, which would limit its thickness below 25 nm for the contact passivation layer.[29] The contact properties induced by this thin film were susceptible to adjacent films, e.g., transparent conductive oxides[17] and metals.[16a,25]

To further improve the passivation and contact property of Si/MoN_x contact and the stability of MoO_x/Ag contact, devices with a dual-hole-selective passivating layer of MoO_x/MoN_x were fabricated. The MoO_x/MoN_x/Ag contact undermined device's V_{oc} and J_{sc} but promoted FF gradually by increasing the thickness of MoN_x film from 0 to 200 nm. The device with a rear contact of MoO_x (20 nm)/MoN_x (10–20 nm)/Ag yielded the champion PCE of 17.2% (Table S4, Supporting Information). Further increasing the thickness of MoN_x film would degrade the performance to the level of the device with MoN_x/Ag contacts. The suppressed J_{sc} was mainly due to the parallel absorption of MoN_x film. The gradually decreased V_{oc} was related to the fact that the thin MoO_x film was susceptible to MoN_x films because the nitrogen signal was observed in MoO_x film in the ToF-SIMS depth profile of MoN_x/MoO_x/Si interfaces (Figure S6, Supporting Information). It is worth noting that the device stability was significantly improved with MoO_x/MoN_x/Ag contact. As shown in Figure 3e, the PCE of the devices with 10 nm thick MoO_x/Ag contacts degraded from 17% to 14% in 3 months, whereas MoO_x/MoN_x/Ag contacts kept the PCE of over 16%, similar stability phenomena were also found in the devices with MoO_x (20 nm)/MoN_x/Ag contact (Figure 3f). The use of MoN_x as rear contact can significantly improve the device's stability.

To confirm MoN_x enabling a silver diffusion barrier, the Ag/MoN_x and Ag/MoO_x interfaces stored in ambient air for 2 months were monitored with ToF-SIMS. The ion intensity of silver showed a sharp attenuation at Ag/MoN_x interface layer (IL) and decreased to the minimum detection limit directly in MoN_x film (**Figure 4**a), whereas the silver can be detected through the whole MoO_x film (Figure 4b), indicating diffusion of silver into MoO_x film.[25] Few silver atoms diffuse into MoN_x film, which results in enhanced PV stability. Apart from the diffusion barrier for silver diffusion, the relatively stable work function of MoN_x also contributes to the device's stability. The work function of MoN_x is less affected by air exposure than MoO_x, as shown in Figure 4c,d. After storing in ambient air for 1 year, the work function of MoN_x (4.60 eV) film became larger than MoO_x (4.36 eV) film. After the Ar gas cluster ion beam (GCIB) cleans contaminated carbon or organics adsorbed

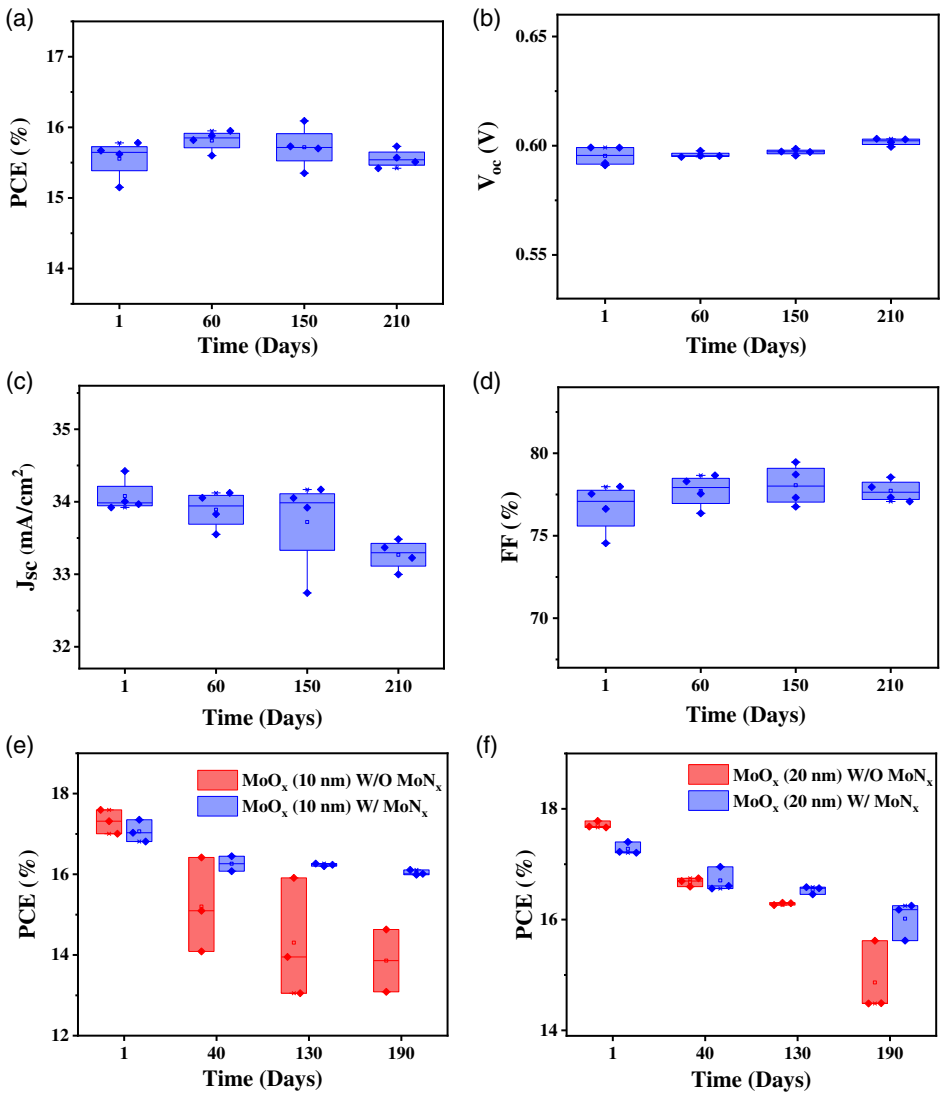

Figure 3. The stability of the devices with the MoN_x hole-selective passivating contact. a) The PCE, b) V_{oc}, c) J_{sc}, and d) FF evolution of devices with 200 nm MoN_x layer in 7 months. e,f) The PCE stability of the devices with MoO_x and MoO_x/MoN_x contacts.

on the surface, the intrinsic work function of MoO_x is only 0.09 eV higher than MoN_x, albeit that the work function of fresh MoO_x (6.8 eV)[15c] is much higher than MoN_x. The work function change in MoN_x (0.72 eV) is much less than MoO_x (1.05 eV) before and after GCIB cleaning, which also reveals that the MoN_x surface adopts better chemical stability than MoO_x.

3. Conclusion

We have demonstrated a stable MoN_x hole-selective passivating contact for efficient and stable silicon solar cells with a cost-effective method. With superior conductivity (resistivity of $5.0 \times 10^{-4}\,\Omega\,cm$) and a higher work function (5.62 eV), MoN_x film as hole-selective passivating layer can achieve a PCE of 15.9%. Although the hole-selective passivation of MoN_x films was inferior to fresh MoO_x films, the device with MoN_x/Ag contacts showed much higher stability than MoO_x/Ag contacts and kept a stable PCE for at least 7 months. Dual hole-selective passivating MoO_x/MoN_x/Ag contacts further improved PCE to 17.2% and retained better stability than MoO_x/Ag contact. The stability induced by MoN_x film was attributed to its barrier for silver diffusion and stable work function compared to MoO_x. Our work provides an alternative idea to develop stable and cost-effective metal nitrides as hole-selective passivating contacts for efficient crystal silicon solar cells.

4. Experimental Section

Preparation and Characterization of MoN_x Film: The MoN_x films were deposited by the direct current (DC) magnetron sputtering method on glass substrates and Si substrates for resistivity and XPS/UPS measurement, respectively. The glass substrate was degreased by ethanol with an ultrasonic cleaner and then rinsed with deionized water. The Si

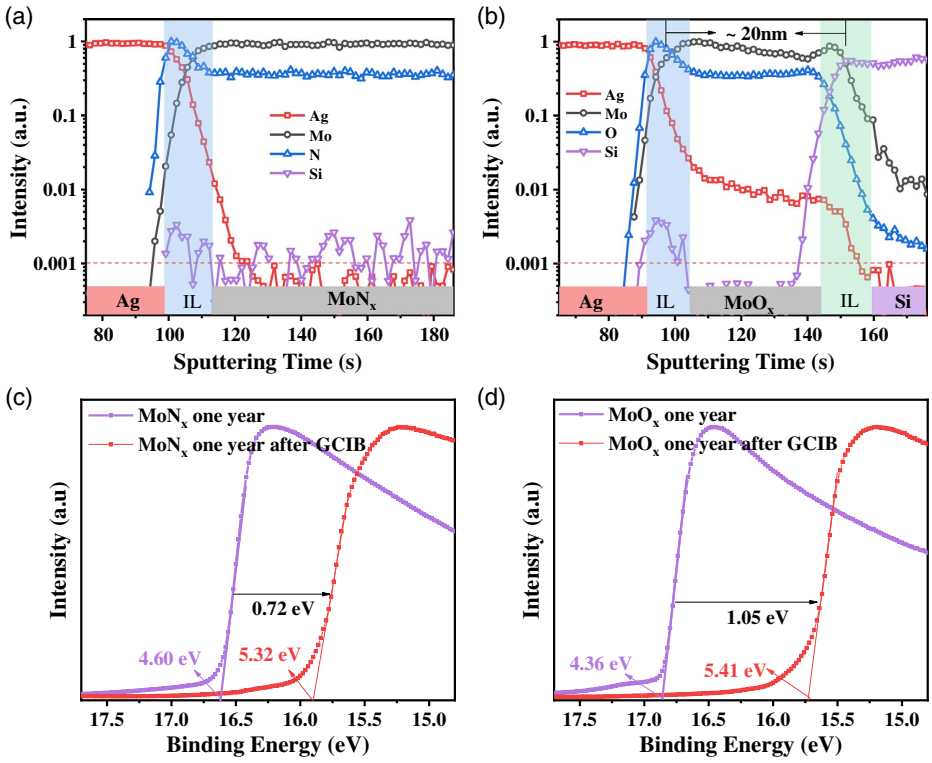

Figure 4. The silver diffusing situation in MoN_x and MoO_x films and work function stability of MoN_x and MoO_x films. a,b) ToF-SIMS depth profile of Ag/MoN_x (a) and Ag/MoO_x (b) IL. The minimum detection limit of silver is marked with a red horizontal line. c,d) The work functions obtained from UPS spectra of MoN_x films (c) and MoO_x (d) films (stored in air for 1 year) before and after Ar GCIB cleaning contaminated carbon or organics adsorbed on the surface.

substrate was ultrasonic degreased by ethanol and rinsed with deionized water, then etched by immerging in a 10% HF solution for 5 min to remove the native oxide layer on the surface. Then, the substrates were dried by blowing with high-pressure nitrogen and loaded into the deposition chamber. The deposition was conducted using a 50.8 mm diameter and 5 mm thickness Mo (99.99% purity) target, and the distance between substrate and target was fixed at 8 cm. The vacuum pressure reached 8.0×10^{-4} Pa before deposition, and the Mo target was first presputtered at 30 W for 10 min to remove any possible oxide layer. During the deposition process, no external heating was applied to the substrate, and the Mo target was sputtered at 60 W. The MoN_x films were deposited in a mixed ambient of N_2 and Ar (the purity of 99.99%) with pressure at 0.5 Pa, and the ratios of gas flow rate between N_2 and Ar were, respectively, 1:1, 1:2, 1:3, and 1:5.

Thickness of MoN_x films was obtained from a KLA-Tencor thickness profilometer. The sheet resistances were measured using the 4-point probe or Hall effect testing instrument HL5500. The crystal structure, work function, and composition of MoN_x films were characterized by XRD (Bruker D8 Discover diffractometer), UPS(PHI 5000 versaprobe II), and XPS (PHI 5000 versaprobe II) measurements. XPS spectra were recorded using 150 W Al Kα radiation (1486.6 eV). All XPS spectra data were referenced to hydrocarbon C1s peak at 284.5 eV. After Shirley background subtraction and fitting by Gaussian–Lorentzian curves, a multipeak deconvolution of the spectra was performed, allowing quantifying the relative content of each oxidation state and the nitrogen to metal(N/M) ratios from the integrated peak areas. The Mo3d peak envelope was deconvoluted according to constraints that the interval between the $Mo3d_{5/2}$ and the $Mo3d_{3/2}$ was kept near 3.15 eV, and the area ratio of the $Mo3d_{5/2}$ and the $Mo3d_{3/2}$ peak was kept near to the theoretical value of 3/2. The area ratios of three kinds of Mo $3p_{3/2}$ peaks with different value states were kept equal to the area ratios of three kinds of Mo $3d_{5/2}$ peaks. The semiquantitative calculation of atomic concentration was according to the formula $\frac{n_i}{n_j} = \frac{I_i}{I_j} \times \frac{\sigma_j}{\sigma_i} \times \frac{E_{k_j}^{0.5}}{E_{k_i}^{0.5}}$,[30] where n is the number of the atoms, I is the area of peak, σ is the photoionization cross section of corresponding atom orbital (for Al Kα, Mo $3d_{5/2} = 5.62$, Mo $3p_{3/2} = 5.94$, N1s = 1.8, O1s = 2.93),[31] E_k is photoelectron kinetic energy, $E_k = h\nu$-BE (for Al Kα, $h\nu = 1486.6$ eV). The UPS was tested with a monochromatized HeI (21.22 eV) excitation source. The Hall effect of MoN_x film on the glass substrate was measured with HL5500. The optical transmittance spectra were obtained by ultraviolet and visible spectrophotometer Lambda 950.

Preparation and Characterization of the Devices: The devices were fabricated on the back surface of p-type silicon with a semi-PERC structure on the front. The semi-PERC structure was prepared on standard 156 mm p-type <100> czochralski (CZ) wafers, and the detailed fabrication process was the same as previous work.[24] The wafers were cut into small pieces with an area of $3.12 \times 3.12\ cm^2$ for device fabrication. Before depositing full area MoN_x rear contact, the back surface of each sample was treated with HF gas for 5 min. After depositing MoN_x film, a silver electrode of 100 nm was evaporated on MoN_x surface. For devices with MoO_x/Ag contact, MoO_x and silver were evaporated in sequence in the same vacuum chamber.

The *J–V* parameters of devices were measured under standard 1 sun condition (100 mW cm^{-2}, AM1.5G spectrum, 25 °C) using an Enlitech solar simulator. The EQE was obtained by the Enlitech quantum efficiency measurement system QE-R 3011. The effective carrier lifetime of silicon wafer passivated with MoN_x film was investigated on MDPmap-Laboratory equipment, Freiberg Instruments. The contact properties of MoN_x and MoO_x on p-type silicon (1–5 Ω cm) were investigated using the method devised by Cox and Strack.[26] Specifically, the test structures

were prepared by depositing circular front electrodes of MoN_x/Ag with different diameters through a shadow mask and evaporating full-area Al (100 nm) at the back to form an ohmic contact. The *J–V* measurement of contact structures was performed on a probe station in a dark environment. Depth profile mass spectra of Ag (100 nm)/MoN_x (200 nm)/Si, Ag (100 nm)/MoO_x (20 nm)/Si and MoN_x (100 nm)/MoO_x (20 nm)/Si structures were conducted on a ToF-SIMS 5-100 instrument (ION-TOF GmbH).

Supporting Information

Supporting Information is available from the Wiley Online Library or from the author.

Acknowledgements

Ya.L. and Yu.L contributed equally to this work. This work was supported by the National Natural Science Foundation of China (91833303, 61974098), the National Key Research and Development Program of China (2016YFA0202402), Jiangsu High Educational Natural Science Foundation (18KJA430012), Jiangsu Key R & D programs (BE2018006-3), China Postdoctoral Science Foundation (2019M651936), the Science and Technology Commission of Shanghai Municipality (19ZR1479100 and 20520760700), and the 111 Program and Collaborative Innovation Center of Suzhou Nano Science and Technology (NANO-CIC). The authors are grateful for the support for Nano-X in Suzhou Institute of Nano-Tech and Nano-Bionics, CAS.

Conflict of Interest

The authors declare no conflict of interest.

Data Availability Statement

The data that support the findings of this study are available from the corresponding author upon reasonable request.

Keywords

hole-selective passivating contacts, low cost, magnetron sputtering deposition, molybdenum nitrides, stability

Received: March 23, 2021
Revised: May 6, 2021
Published online:

[1] T. G. Allen, J. Bullock, X. Yang, A. Javey, S. De Wolf, *Nat. Energy* **2019**, *4*, 914.
[2] B. Min, M. Müller, H. Wagner, G. Fischer, R. Brendel, P. P. Altermatt, H. Neuhaus, *IEEE J. Photovoltaics* **2017**, *7*, 1541.
[3] A. Richter, S. W. Glunz, F. Werner, J. Schmidt, A. Cuevas, *Phys. Rev. B* **2012**, *86*, 165202.
[4] a) S. C. Baker-Finch, K. R. McIntosh, D. Yan, K. C. Fong, T. C. Kho, *J. Appl. Phys.* **2014**, *116*, 063106; b) D. Yan, A. Cuevas, *J. Appl. Phys.* **2014**, *116*, 194505; c) D. Yan, A. Cuevas, *J. Appl. Phys.* **2013**, *114*, 044508.
[5] A. Richter, M. Hermle, S. W. Glunz, *IEEE J. Photovoltaics* **2013**, *3*, 1184.
[6] a) K. Masuko, M. Shigematsu, T. Hashiguchi, D. Fujishima, M. Kai, N. Yoshimura, T. Yamaguchi, Y. Ichihashi, T. Mishima, N. Matsubara, T. Yamanishi, T. Takahama, M. Taguchi, E. Maruyama, S. Okamoto, *IEEE J. Photovoltaics* **2014**, *4*, 1433; b) K. Yoshikawa, H. Kawasaki, W. Yoshida, T. Irie, K. Konishi, K. Nakano, T. Uto, D. Adachi, M. Kanematsu, H. Uzu, K. Yamamoto, *Nat. Energy* **2017**, *2*, 17032.
[7] a) A. Richter, J. Benick, F. Feldmann, A. Fell, M. Hermle, S. W. Glunz, *Sol. Energy Mater. Sol. Cells* **2017**, *173*, 96; b) C. Hollemann, F. Haase, S. Schäfer, J. Krügener, R. Brendel, R. Peibst, *Prog. Photovoltaics: Res. Appl.* **2019**, *27*, 950.
[8] J. Schmidt, R. Peibst, R. Brendel, *Sol. Energy Mater. Sol. Cells* **2018**, *187*, 39.
[9] a) W. Wang, J. He, D. Yan, C. Samundsett, S. P. Phang, Z. Huang, W. Shen, J. Bullock, Y. Wan, *Sol. Energy Mater. Sol. Cells* **2020**, *206*, 110291; b) X. Yang, Q. Bi, H. Ali, K. Davis, W. V. Schoenfeld, K. Weber, *Adv. Mater.* **2016**, *28*, 5891.
[10] a) Y. Wan, S. K. Karuturi, C. Samundsett, J. Bullock, M. Hettick, D. Yan, J. Peng, P. R. Narangari, S. Mokkapati, H. H. Tan, C. Jagadish, A. Javey, A. Cuevas, *ACS Energy Lett.* **2018**, *3*, 125; b) G. Chistiakova, B. Macco, L. Korte, *IEEE J. Photovoltaics* **2020**, *10*, 398.
[11] X. Yang, H. Xu, W. Liu, Q. Bi, L. Xu, J. Kang, M. N. Hedhili, B. Sun, X. Zhang, S. De Wolf, *Adv. Electron. Mater.* **2020**, *6*, 2000467.
[12] a) J. Bullock, M. Hettick, J. Geissbühler, A. J. Ong, T. Allen, C. M. Sutter-Fella, T. Chen, H. Ota, E. W. Schaler, S. De Wolf, C. Ballif, A. Cuevas, A. Javey, *Nat. Energy* **2016**, *1*, 15031; b) J. Bullock, A. Cuevas, T. Allen, C. Battaglia, *Appl. Phys. Lett.* **2014**, *105*, 232109.
[13] a) L. G. Gerling, S. Mahato, A. Morales-Vilches, G. Masmitja, P. Ortega, C. Voz, R. Alcubilla, J. Puigdollers, *Sol. Energy Mater. Sol. Cells* **2016**, *145*, 109; b) H. Lin, D. Ding, Z. Wang, L. Zhang, F. Wu, J. Yu, P. Gao, J. Ye, W. Shen, *Nano Energy* **2018**, *50*, 777; c) D. Zielke, A. Pazidis, F. Werner, J. Schmidt, *Sol. Energy Mater. Sol. Cells* **2014**, *131*, 110.
[14] J. Schmidt, V. Titova, D. Zielke, *Appl. Phys. Lett.* **2013**, *103*, 183901.
[15] a) M. T. Greiner, L. Chai, M. G. Helander, W.-M. Tang, Z.-H. Lu, *Adv. Funct. Mater.* **2012**, *22*, 4557; b) J. Meyer, K. Zilberberg, T. Riedl, A. Kahn, *J. Appl. Phys.* **2011**, *110*, 033710; c) Irfan, H. Ding, Y. Gao, C. Small, D. Y. Kim, J. Subbiah, F. So, *Appl. Phys. Lett.* **2010**, *96*, 243307.
[16] a) M. T. Greiner, L. Chai, M. G. Helander, W.-M. Tang, Z.-H. Lu, *Adv. Funct. Mater.* **2013**, *23*, 215; b) L. G. Gerling, C. Voz, R. Alcubilla, J. Puigdollers, *J. Mater. Res.* **2016**, *32*, 260.
[17] J. Geissbühler, J. Werner, S. Martin de Nicolas, L. Barraud, A. Hessler-Wyser, M. Despeisse, S. Nicolay, A. Tomasi, B. Niesen, S. De Wolf, C. Ballif, *Appl. Phys. Lett.* **2015**, *107*, 081601.
[18] L. E. Black, B. W. H. van de Loo, B. Macco, J. Melskens, W. J. H. Berghuis, W. M. M. Kessels, *Sol. Energy Mater. Sol. Cells* **2018**, *188*, 182.
[19] X. Yang, W. Liu, M. De Bastiani, T. Allen, J. Kang, H. Xu, E. Aydin, L. Xu, Q. Bi, H. Dang, E. AlHabshi, K. Kotsovos, A. AlSaggaf, I. Gereige, Y. Wan, J. Peng, C. Samundsett, A. Cuevas, S. De Wolf, *Joule* **2019**, *3*, 1314.
[20] X. Yang, E. Aydin, H. Xu, J. Kang, M. Hedhili, W. Liu, Y. Wan, J. Peng, C. Samundsett, A. Cuevas, S. De Wolf, *Adv. Energy Mater.* **2018**, *8*, 1800608.
[21] a) I. Jauberteau, A. Bessaudou, R. Mayet, J. Cornette, J. L. Jauberteau, P. Carles, T. Merle-Méjean, *Coatings* **2015**, *5*, 656; b) V. P. Anitha, A. Bhattacharya, N. G. Patil, S. Major, *Thin Solid Films* **1993**, *236*, 306.
[22] H. Matsuhashi, S. Nishikawa, *Jpn. J. Appl. Phys.* **1994**, *33*, 1293.
[23] Y. Wang, R. Y. Lin, *Mater. Sci. Eng.: B* **2004**, *112*, 42.

[24] a) Y. L. Jeyachandran, S. K. Narayandass, D. Mangalaraj, S. Areva, J. A. Mielczarski, *Mater. Sci. Eng.: A* **2007**, *445–446*, 223; b) M. Wittmer, B. Studer, H. Melchior, *J. Appl. Phys.* **1981**, *52*, 5722.
[25] S. Cao, J. Li, Y. Lin, T. Pan, G. Du, J. Zhang, L. Yang, X. Chen, L. Lu, N. Min, M. Yin, D. Li, *Sol. RRL* **2019**, *3*, 1900274.
[26] R. H. Cox, H. Strack, *Solid-State Electron.* **1967**, *10*, 1213.
[27] R. T. Tung, *Appl. Phys. Rev.* **2014**, *1*, 011304.
[28] a) J. D. McBrayer, R. M. Swanson, T. W. Sigmon, *J. Electrochem. Soc.* **1986**, *133*, 1242; b) T. C. Nason, G. R. Yang, K. H. Park, T. M. Lu, *J. Appl. Phys.* **1991**, *70*, 1392.
[29] C. Battaglia, S. M. de Nicolás, S. De Wolf, X. Yin, M. Zheng, C. Ballif, A. Javey, *Appl. Phys. Lett.* **2014**, *104*, 113902.
[30] Y. Boudeville, F. Figueras, M. Forissier, J.-L. Portefaix, J. C. Vedrine, *J. Catal.* **1979**, *58*, 52.
[31] J. H. Scofield, *J. Electron. Spectrosc. Relat. Phenom.* **1976**, *8*, 129.